Letter Vol. 43, No. 6 / 15 March 2018 / Optics Letters 1331

Optics Letters

Transverse translation diverse phase retrieval using soft-edged illumination

AARON M. MICHALKO* AND JAMES R. FIENUP

The Institute of Optics, University of Rochester, Rochester, New York 14627, USA
**Corresponding author: aaron.michalko@rochester.edu*

Received 22 January 2018; revised 13 February 2018; accepted 14 February 2018; posted 15 February 2018 (Doc. ID 319971); published 14 March 2018

Transverse translation diverse phase retrieval (TTDPR), a ptychographic image-based wavefront-sensing technique, is a viable method for optical shop testing due to its high accuracy and relatively simple experimental arrangement. However, when measuring a reflective optic, a normally hard-edged translating illumination will become soft-edged due to diffraction, which may reduce the accuracy of TTDPR by suppressing fine structures in measured data. In this Letter, we quantitatively explore the wavefront-sensing accuracy of TTDPR in the presence of soft-edged translating illumination.

OCIS codes: (100.5070) Phase retrieval; (120.3940) Metrology; (120.5050) Phase measurement.

https://doi.org/10.1364/OL.43.001331

Transverse translation diverse phase retrieval (TTDPR) [1–4] is an image-based wavefront-sensing technique similar to the coherent diffractive imaging technique (CDI) of ptychography [5–9]. In TTDPR, the unknown phase of an optical field of interest is reconstructed based on intensity-only measurements taken in a plane positioned a distance from the field of interest, often near focus. A known subaperture illumination is transversely translated across a field of interest, and intensities are recorded on an array detector for each translated illumination position. These data are then used in an iterative phase retrieval algorithm to reconstruct the amplitude and phase of the field of interest. TTDPR has been proposed before as a method for as-built hardware characterization of optical systems [2,3,5,10].

TTDPR is an attractive method for optical shop testing due to its relatively simple experimental arrangement [1]. For certain test configurations, such as a concave surface in reflection or a positive-powered optic in transmission, TTDPR may require only a translating aperture and an array detector to determine the wavefront aberration function of an optic under test, from which surface topography can also be inferred. Due to the lack of complexity in the TTDPR test geometries, TTDPR is relatively inexpensive compared to a conventional interferometer. Unlike interferometry, certain types of optics can be measured using TTDPR without requiring any reference optics, thereby reducing system cost and eliminating induced aberration from these additional optics. TTDPR does not suffer from retrace errors, allowing aspheric wavefronts, whose wavefront departures would create unresolvable fringes in an interferogram, to be measured without requiring custom null optics [11], thus making TTDPR suitable for aspheric and freeform metrology. Furthermore, because TTDPR does not rely on the interference between a test and reference beam, it has reduced sensitivity to vibration that degrades the accuracy of interferometers.

The specific test geometry of a TTDPR system depends on the type of measurement being performed. If it is used to characterize the transmitted wavefront error, the full aperture of a test optic can be illuminated, and a hard-edged subaperture may be placed just before or after the optic to create a translating illumination pattern. Such a measurement was demonstrated by Brady [1]. Measurements of surface error, however, must be taken in reflection. A hard-edged translating mask cannot be placed directly in the pupil for a reflective measurement because it may contact and, therefore, harm the reflective surface or obscure regions of the reflected field, as illustrated in Fig. 1(a). One way to overcome this limitation is instead to optically project a known illumination pattern onto the surface of interest. Due to diffraction effects, an illumination pattern created by a distant hard-edged mask will have softened edges when incident on the optical surface, the exact nature of which depends on the source wavelength, mask size, and propagation distance to the surface. In this context, we define softness as a smooth variation from high amplitude to low, near the edge of the illumination pattern.

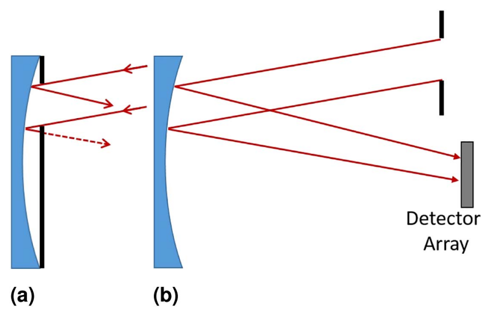

Fig. 1. TTDPR for reflective surface metrology. (a) Mask near the surface of interest may obscure reflected intensity and (b) a solution to project instead the illumination pattern from a distance.

A soft-edged support constraint in image-reconstruction phase retrieval, which is analogous to soft-edged illumination in TTDPR, has been shown to cause degradation in reconstructed images, even in noiseless simulations [12]. For that reason, in this Letter, we explore the wavefront-sensing accuracy of TTDPR for optical metrology in the presence of a soft-edged illumination pattern through computer simulation. Softness in the illumination suppresses, in the measured intensities, fine fringe structures that are thought to help phase retrieval algorithms converge to a unique solution. Although TTDPR with soft-edged illumination has been demonstrated for CDI [4], the object, a simulated biological specimen, had rapidly changing features throughout its area, which created large amounts of diffractive structure in the far field, even in the presence of soft-edged illumination. This differs from the case of optical metrology, in which the reconstructed object, a reflected wavefront, is assumed to be dominated by slowly varying phase terms. The fine diffractive structure from hard-edged illumination may be more important in optical metrology than in CDI, motivating our investigation.

The computational forward model used for TTDPR is as follows. We first modeled the field as

$$h(x,y) = |h(x,y)| \exp[i2\pi W(x,y)], \tag{1}$$

where $W(x,y)$ is the classical wavefront aberration function of the field, having units of waves. For the TTDPR simulations in this Letter, $W(x,y)$ was constructed as a weighted superposition of J Zernike polynomials [13]:

$$W(x,y) = \sum_{j=1}^{J} a_j Z_j(x,y), \tag{2}$$

where the a_j is the weighting coefficient of the jth Zernike polynomial. A known subaperture illumination, $A(x,y)$, which can be complex-valued, was transversely translated across the field, resulting in a transmitted field:

$$g_n(x,y) = A(x - x_n, y - y_n)h(x,y) \tag{3}$$

for each of n translated positions [1]. In this Letter, integer pixel nominal translations (x_n, y_n) were used to simulate synthetic test data, and bilinear interpolation was used for subpixel translation if (x_n, y_n) were varying as optimization parameters [3].

Next, $g_n(x,y)$ was digitally propagated to the detector plane by

$$G_n(u,v) = \boldsymbol{P}[g_n(x,y)], \tag{4}$$

where $\boldsymbol{P}$ is a propagator for the system. In the absence of noise, the intensity distribution measured by the array detector was given by

$$D_n(u,v) = |G_n(u,v)|^2. \tag{5}$$

These data were then used in an iterative phase retrieval algorithm. In each iteration, a candidate wavefront $\hat{W}(x,y)$ was constructed, and intensities were simulated according to Eqs. (1)–(5). These simulated intensities were compared to measured data using a normalized least-squares error metric:

$$E = \frac{\sum_n \sum_{u,v} w_n(u,v)[M_n(u,v) - D_n(u,v)]^2}{\sum\limits_n \sum\limits_{u,v} [D_n(u,v)]^2}, \tag{6}$$

where $w_n(u,v)$ is a weighting function, and $M_n(u,v)$ is the nth modeled intensity, given by

$$M_n(u,v) = \beta_n |G_n(u,v)|^2 + \delta_n. \tag{7}$$

β_n and δ_n are per-frame linear detector gain and bias, respectively, with values calculated according to Eq. (C3) in [2] to make Eq. (6) gain and bias invariant. E was then minimized with respect to experimental parameters to yield a final estimate of $W(x,y)$. Exact algorithmic gradients for this type of forward model were calculated and used for non-linear optimization using the L-BFGS algorithm [14,15].

Simulations were performed to explore the wavefront-sensing accuracy of TTDPR in the presence of soft-edged translating illumination. In each simulation, the field magnitude, $|h(x,y)|$, was modeled by a binary circular subaperture, over which a set of orthonormal Zernike polynomials were defined. 35 Zernike polynomials were superposed to model $W(x,y)$ with randomly generated coefficients, a_j. Because we expect real-life wavefronts to be dominated by lower-order terms, such as astigmatism and coma, wavefront coefficients were multiplied by a function which decreases in value as polynomial order increases. Then, for each simulation, the root-mean-square (RMS) value of $W(x,y)$ was scaled to a prescribed value.

For these simulations, the soft-edged illumination was modeled using the raised cosine function

$$A(\rho) = \begin{cases} 1, & 0 < \rho \le R\left(\frac{1-\beta}{1+\beta}\right) \\ \frac{1}{2}\left\{1 + \cos\left[\frac{\pi(1+\beta)}{2\beta}\left(\frac{\rho}{R} - \frac{1-\beta}{1+\beta}\right)\right]\right\}, & R\left(\frac{1-\beta}{1+\beta}\right) < \rho \le R \\ 0, & R < \rho \end{cases} \tag{8}$$

where

$$\rho = \rho(x,y) = \sqrt{x^2 + y^2}, \tag{9}$$

and R is the radius of A.

The parameter β, which ranges in value from 0 to 1, tunes the relative "softness" of A, as shown in Fig. 2. For $\beta = 0$, $A(x,y)$ is a hard-edged circle with radius R. For $\beta = 1$, $A(x,y)$ is a radially symmetric truncated cosine cycle with period $2R$. Values of β between 0 and 1 approximate smoothly varying illumination patterns that may arise in the lab from beam diffraction from a clipping subaperture. For example, $\beta = 1$ roughly approximates the amplitude from a circular aperture propagated with a Fresnel number [16] $N_f = 1$, $\beta = 0.5$ to $N_f = 10$, and $\beta = 1/7$ to $N_f = 100$. These patterns also approximate other illumination strategies, such as the use of beam shaping optics. The parametrization of $A(x,y)$ is also selected so that the total non-zero support of $A(x,y)$ is constant for all simulated values of β. Therefore, even when β is varied between simulations, the total footprint of all translated illuminations will experience the same simulated field. 32 translated positions, (x_n, y_n), were used in each

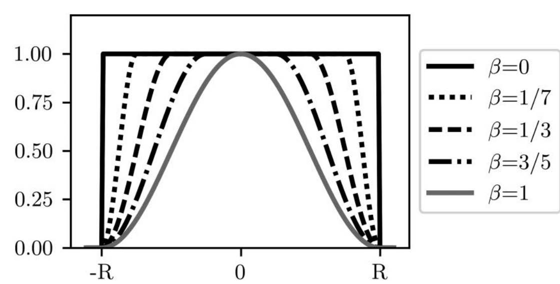

Fig. 2. One-dimensional cut-through of raised cosine illumination, according to Eq. (8), for various values of β.

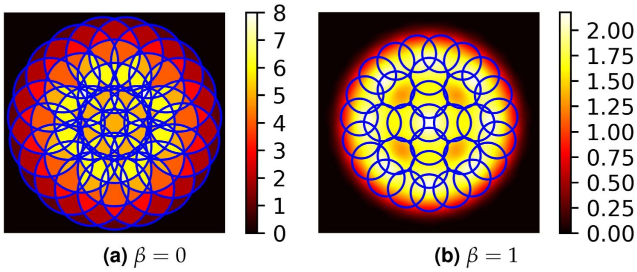

Fig. 3. Translated illumination patterns used for TTDPR simulations. Each circle indicates the region of >50% peak amplitude; the color indicates the sum of all translated illumination (amplitude). Note that as β increased, the pupil was both effectively apodized and sampled more sparsely.

simulation. A visualization of all translated illumination patterns is shown in Fig. 3. In order to isolate the effect of varying β, the illumination was translated such that it never overlapped the edge of $|h(x, y)|$. Otherwise, the hard edges would have been induced into otherwise smooth illumination patterns. The peak of each simulated intensity measurement was scaled to 40,000 photo-electrons, and Poisson noise and 16-electron RMS Gaussian read noise were added, the noise characteristics being indicative of a reasonable-quality CCD camera.

First, simulations were performed to reconstruct a 0.10-wave RMS wavefront (piston, tilt, and power removed), which corresponds to the wavefront aberration of a well-corrected optic. A known amount of 10-wave peak-to-valley defocus was added to the field wavefront, because it has been shown that phase retrieval for wavefront sensing can benefit from the addition of defocus to the nominal wavefront [17–20]. For each of five β values, TTDPR simulations were performed on 10 different wavefront realizations, assuming that all experimental parameters except $W(x, y)$ were known. Figure 4 shows the results of this set of simulations: the RMS wavefront-sensing error (WFSE) as a function of β. The WFSE is in units of waves, calculated as an equally weighted RMS difference between the reconstructed and known wavefronts over the non-zero footprint of all $A(x - x_n, y - y_n)$. We defined a success criterion of 0.015 waves of RMS WFSE to identify successful reconstructions. All results shown in Fig. 4 meet the success criterion, with WFSE <1/1000 waves for all β. Although median WFSE tends to increase with β, WFSE caused by beam softness alone should not impose a practical constraint in an optical shop-testing environment for well-corrected optics,

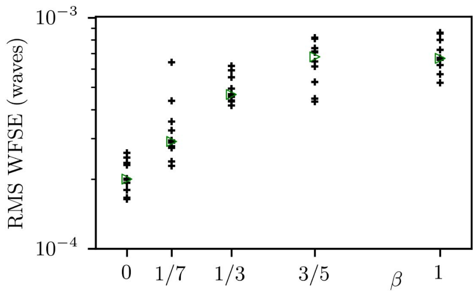

Fig. 4. RMS WFSE versus β for wavefront reconstructions with 0.10-wave RMS. Black +, final WFSE for each of 10 randomly generated wavefronts; green ▷, median WFSE.

where other sources of laboratory error will likely set the lower limit of overall measurement uncertainty.

Next, simulations were performed to reconstruct fields with ~10-wave RMS wavefront aberration. These simulations correspond to the measurement of an aspheric or freeform optical surface, in which the surface departure will induce large aberrations in the reflected field. A wavefront $\hat{W}(x, y)$ with 3.0 wave RMS departure from the true wavefront was used as a starting point for optimization. $\hat{W}(x, y)$ in this case corresponds to the expected wavefront from a given nominal surface prescription, and the true wavefront corresponds to one manufactured having unknown fabrication errors. We note that this set of simulation parameters created a more difficult case for TTDPR, due to both larger nominal aberrations and a larger distance between the starting point and true solution for optimization.

After an initial round of simulations, it was discovered that some intensities were being aliased by the discrete Fourier transform (DFT) used for digital propagation [Eq. (4)]. Figure 5 illustrates one worst case. The DFT is periodic, and significant aliasing occurs when the wavefront function varies too rapidly between adjacent pixels. A phase change of π radians/pixel, or 0.5 waves/pixel, will result in energy at the edge of the simulated detector window. As a rule of thumb, one should keep wavefront slopes $< \pi$ rad/pixel so that the simulated detector window contains all significant energy, i.e.,

$$|\boldsymbol{W}_{p,q} - \boldsymbol{W}_{p+1,q}| < \pi, \tag{10}$$

$$|\boldsymbol{W}_{p,q} - \boldsymbol{W}_{p,q+1}| < \pi, \tag{11}$$

for all values of p and q, for the p, q pixel-indexed wavefront array, $\boldsymbol{W}$. For a given wavefront realization, this is achieved by simply increasing the number of pixels across $\boldsymbol{W}$. In practice, one should be cautious when using phase retrieval with data gathered from the lab, so that non-physical aliasing does not hinder the ability of phase retrieval to match the physical data.

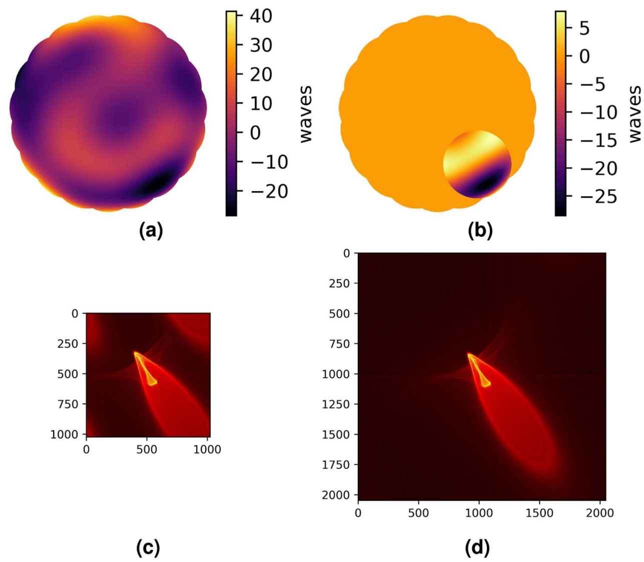

Fig. 5. (a) Sample aberrated wavefront. (b) Instantaneous wavefront for a given subaperture with $\beta = 0$. (c) Resulting intensity, raised to the 1/5th power. Aliasing occurs at the corners of the simulated detector due to periodicity in the DFT. (d) Intensity raised to the 1/5th power after doubling pupil resolution.

After correcting the aliased intensities by doubling the number of pixels over the wavefront, all reconstructions met the success criterion of RMS WFSE <0.015 waves, as shown in Fig. 6. Although WFSE tended to be larger than the results with less aberrated wavefronts, shown in Fig. 4, excellent performance was attainable for all values of β, indicating that beam softness by itself should not be a limiting factor in TTDPR accuracy on highly aberrated wavefronts. If one desires even higher wavefront-sensing accuracy, steps can be taken to mitigate residual WFSE, including increasing the overlap between adjacent subapertures, improving the signal-to-noise ratio by averaging multiple measured intensities for each subaperture position, and by only considering WFSE over regions which were sampled by multiple subapertures.

After investigating the performance of TTPDR when all experimental parameters are known except $W(x, y)$, we performed additional simulations, including uncertainty in subaperture translation. Such uncertainty might arise from incorrect calibration of a TTDPR system, or from positioning errors in the stages used to translate the illumination. Random translation errors were drawn from a uniform distribution with a standard deviation of $R/50$ and added to the nominal translations to form an initial guess for (x_n, y_n). In optimization, iterations were first performed varying only Zernike wavefront coefficients. Next, iterations were performed varying wavefront coefficients along with translations (x_n, y_n). Figure 7 shows the results of TTDPR simulations on 0.1-wave RMS wavefronts. In order to correct for any shared global linear phase, which would apply only a common shift to all simulated intensities, WFSE was calculated with piston and tilt removed. Compared to the results in Fig. 4, the results in Fig. 7 have both higher median and variance for each β, which we attribute to the effect of unknown translation [2]. However, all reconstructions readily satisfy the success criterion of WFSE <0.015 waves, indicating that limited translation knowledge should not be the dominant source of wavefront sensing error for measuring well-corrected optics. For higher aberrated wavefronts, we expect that small translation errors can be tolerated by TTDPR, though performance may depend on the aberration content, subaperture pattern, etc., and is not explored in this initial Letter.

In conclusion, we have explored the wavefront-sensing accuracy of TTDPR, a viable technique for optical surface metrology, in the presence of soft-edged translating illumination. For reconstructions of well-corrected wavefronts, we demonstrated wavefront reconstructions WFSE <0.002 waves RMS, even in the presence of minor unknown translation errors and realistic detector noise. For testing of more aberrated wavefronts, we obtained successful reconstructions (WFSE <0.015-wave RMS) of 10-wave RMS wavefronts for all values of β. The cases of $\beta < 1/7$ are most pertinent to a laboratory application of TTDPR, where we expect some beam softness due to diffraction, but that the illumination is still approximated well by a geometric projection of the translating mask onto the optical surface. For these cases, TTDPR consistently performs very well.

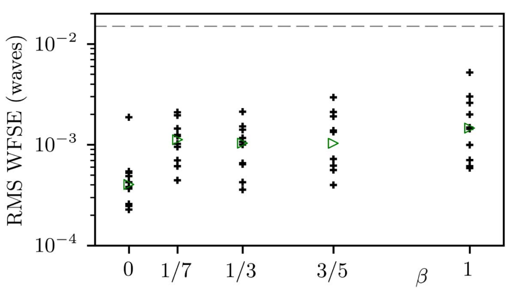

Fig. 6. RMS WFSE versus β for wavefront reconstructions with ~10-wave RMS. Black +, final WFSE for each of 10 randomly generated wavefronts; green ▷, median WFSE. The dashed line shows WFSE success criteria of 0.015 waves.

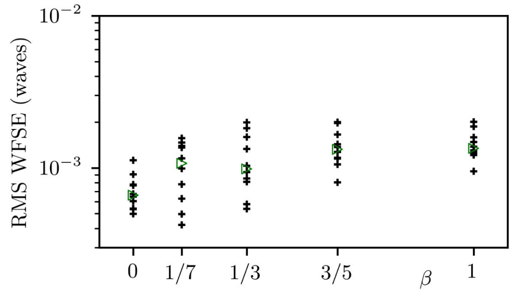

Fig. 7. RMS WFSE versus β for wavefront reconstruction with 0.10-wave RMS when the illumination translation is not well known. Black +, final WFSE for each of 10 randomly generated wavefronts; green ▷, median WFSE.

Funding. National Science Foundation (NSF) I/UCRC Center for Freeform Optics (IIP-1338877, IIP-1338898).

Acknowledgment. The authors thank Dustin Moore, whose phase retrieval library "pharet" was used to perform simulations in this Letter.

REFERENCES

1. G. R. Brady, M. Guizar-Sicairos, and J. R. Fienup, Opt. Express **17**, 624 (2009).
2. D. B. Moore and J. R. Fienup, Appl. Opt. **55**, 2526 (2016).
3. D. B. Moore and J. R. Fienup, Appl. Opt. **55**, 4596 (2016).
4. M. Guizar-Sicairos and J. R. Fienup, Proc. SPIE **7076**, 70760A (2008).
5. C. M. Kewish, M. Guizar-Sicairos, C. Liu, J. Qian, B. Shi, C. Benson, A. M. Khounsary, J. Vila-Comamala, O. Bunk, J. R. Fienup, A. T. Macrander, and L. Assoufid, Opt. Express **18**, 23420 (2010).
6. M. Guizar-Sicairos and J. R. Fienup, Opt. Express **16**, 7264 (2008).
7. H. M. L. Faulkner and J. M. Rodenburg, Phys. Rev. Lett. **93**, 023903 (2004).
8. J. M. Rodenburg and H. M. L. Faulkner, Appl. Phys. Lett. **85**, 4795 (2004).
9. F. Zhang, I. Peterson, J. Vila-Comamala, A. Diaz, F. Berenguer, R. Bean, B. Chen, A. Menzel, I. K. Robinson, and J. M. Rodenburg, Opt. Express **21**, 13592 (2013).
10. T. P. Zielinski and J. R. Fienup, in *Frontiers in Optics*, OSA Technical Digest (CD) (Optical Society of America, 2009), paper SWA2.
11. G. R. Brady and J. R. Fienup, Appl. Opt. **48**, 442 (2009).
12. R. G. Paxman, J. R. Fienup, and J. T. Clinthorne, Proc. SPIE **828**, 184 (1988).
13. R. J. Noll, J. Opt. Soc. Am. **66**, 207 (1976).
14. A. S. Jurling and J. R. Fienup, J. Opt. Soc. Am. A **31**, 1348 (2014).
15. C. Zhu, R. Byrd, P. Lu, and J. Nocedal, ACM Trans. Math. Softw. **23**, 550 (1997).
16. J. W. Goodman, *Introduction to Fourier Optics*, 4th ed. (Macmillan, 2016).
17. J. R. Fienup, B. J. Thelen, R. G. Paxman, and D. A. Carrara, Proc. SPIE **3353**, 930 (1998).
18. B. H. Dean and C. W. Bowers, J. Opt. Soc. Am. A **20**, 1490 (2003).
19. J. R. Fienup, J. C. Marron, T. J. Schulz, and J. H. Seldin, Appl. Opt. **32**, 1747 (1993).
20. J. R. Fienup, Appl. Opt. **32**, 1737 (1993).